Eur. Phys. J. D (2021) 75:310
https://doi.org/10.1140/epjd/s10053-021-00326-x

THE EUROPEAN PHYSICAL JOURNAL D

Regular Article – Atomic and Molecular Collisions

Electronic excitation of benzene by low energy electron impact and the role of higher lying Rydberg states

Alan Guilherme Falkowski[1], Romarly F. da Costa[2,a], Fábris Kossoski[3,b], Michael J. Brunger[4,5], and Marco A. P. Lima[1]

[1] Instituto de Física "Gleb Wataghin", Universidade Estadual de Campinas, 13083-859, Campinas, São Paulo, Brazil
[2] Centro de Ciências Naturais e Humanas, Universidade Federal do ABC, 09210-580, Santo André São Paulo, Brazil
[3] Laboratoire de Chimie et Physique Quantiques (UMR 5626), Université de Toulouse, CNRS, UPS, 31062 Toulouse, France
[4] College of Science and Engineering, Flinders University, Adelaide, Australia
[5] Department of Actuarial Science and Applied Statistics, Faculty of Business and Information Science, UCSI University, Kuala Lumpur 56000, Malaysia

Received 15 October 2021 / Accepted 6 December 2021 / Published online 20 December 2021

Abstract. Benzene is undoubtedly one of the most studied target molecules in electron scattering experiments and calculations. However, there is still a huge knowledge gap on the electronic excitation cross sections of this fundamental collision. Here, we report calculated differential and integral cross sections for elastic and electronic excitation, as well as total cross sections, for electron scattering by the benzene molecule, for impact energies in the 10–50 eV range. We have employed the Schwinger multichannel method, in two levels of approximation. By including extra diffuse functions in the second calculation, the role of higher lying Rydberg states in the multichannel coupling scheme was assessed. We found that such states have minor effects on the elastic and total cross sections. In contrast, the electronic excitation cross sections of the lower-lying bands decrease in magnitude when accounting for the higher Rydberg states, and this effect becomes more pronounced at lower impact energies. Our computed elastic cross sections are in quite good agreement with the available experimental data, whereas the comparison for the electronic excitation channels is still satisfactory. We also discuss the need for accurate excitation energies in order to properly compare theoretical and experimental electronic excitation cross sections.

1 Introduction

This paper is in honor of Prof. Vincent McKoy. He was responsible for the creation of the Brazilian "Schwinger strategy" community for electron–molecule scattering. He came to Brazil in the 1970s and created very strong scientific and friendship bonds. He was a great scientist and advisor, always pointing out the most interesting problems in the field and extracting the best from his students, postdocs, and collaborators. MAPL was his PhD student, A. G. Falkowski and R. F. da Costa are his scientific grandchildren, and F. Kossoski is his scientific grand-grandchild. M. Brunger, not a Brazilian, acknowledges very many interesting and fruitful discussions with Prof. McKoy during their collaboration.

Benzene (C_6H_6) is the simplest member of an important class of compounds known as aromatic hydrocarbons. It consists of six carbon atoms joined together in a ring, with a hydrogen atom bonded to each carbon. Due to its highly symmetric structure and unique properties, benzene has long been considered as a prototype model to investigate the behavior of more complex molecular systems. In particular, studies involving the scattering of low-energy electrons by benzene can provide relevant information about the molecular mechanisms behind bond breaking of the nitrogenous bases in DNA which, in turn, could be helpful for the design of new drugs for chemoradiotherapy [1–3].

Electron collisions with benzene have been the subject of a number of studies, which are summarized below in chronological order. From the theoretical side, early calculations were performed by Read and Whiterod [4] using the Born approximation so as to provide differential cross sections (DCS) and integral cross sections (ICS) for inelastic electron scattering. Lassettre et al. [5] performed measurements and theoretical calculations to investigate the lowest excited states of benzene. Compton et al. measured the electron impact threshold excitation spectrum between 33 and 100 eV [6]. Later, Doering [7,8], through the use of the electron energy loss spectroscopy (EELS) technique, reported good agreement with previous results. Electron transmission experiments carried out by Mathur and Hasted,

[a] e-mail: roma@ifi.unicamp.br
[b] e-mail: fkossoski@irsamc.ups-tlse.fr (corresponding author)

to study resonant features in the total cross sections (TCS) of electrons scattered by benzene, revealed the formation of four temporary negative ion states as structures centered at the energies of 1.10, 2.80, 4.93, and 8.85 eV in the transmitted current [9]. Relative elastic DCS have been measured by Mahant Shetty and coworkers [10], for incident energies of 300, 500, 700, and 900 eV and for scattering angles between 30° and 120°, and were compared with independent atom model (IAM) calculations where only the static interaction was taken into account. These authors found that the higher the incident energy, the better was the observed agreement between experiment and theory. Absolute TCS for electron scattering on benzene molecules have been measured in two distinct electron-transmission experiments, for impact energies between 0.6 eV and 3.5 keV, by Mozejko et al. [11]. By solving the scattering equations with the use of a parameter-free exact-static-exchange plus-correlation-polarization potential to treat the electron–molecule interaction, Gianturco and Lucchese [12] examined the presence of one-electron resonances and also computed DCS and TCS for electron collisions with benzene. Absolute DCS measurements for elastic electron scattering from benzene were reported by Gulley and Buckman [13] for incident energies of 8.5 and 20 eV. By employing the Schwinger multichannel (SMC) method, Bettega et al. presented elastic cross sections for low-energy electron scattering by benzene obtained at the static-exchange (SE) and static-exchange plus polarization (SEP) levels of approximation [14]. Jiang et al. used the additivity rule (AR) and the energy-dependent geometric additivity rule (EGAR) approaches to calculate TCS for a set of molecules including benzene [15]. Cho et al. [16,17] measured the elastic electron scattering cross sections in the energy range from 1.1 to 40 eV. Direct measurements of electron attachment to benzene using Rydberg atom techniques were performed by Field et al. [18]. The scattering cross sections obtained in that work rise sharply at electron impact energies below ∼200 meV, with this being interpreted in terms of the existence of a virtual state. Carsky et al. [19] used the discrete momentum representation (DMR) method to study the elastic scattering of electrons from benzene and observed that the calculated DCS were in good accord, on an absolute scale, with experimental data of the measured angular intensities. Sun and coworkers proposed a modified formulation of the AR to calculate the TCS for electron scattering by benzene, in the range of impact energies from 10 to 2 keV [20]. TCS have been measured using the linear transmission time-of-flight method and were presented by Makochekanwa et al. [21] in the energy range from 0.4 to 1 keV, and by Kimura *et al.* [22] for energies below 500 meV. Absolute elastic DCS at the energy of 1 keV and absolute DCS for the $1^1A_g \rightarrow 1^1B_{1u} + 1^1E_{1u}$ electronic transitions in benzene were reported by Boechat-Roberty et al. [23]. TCS were calculated by De-Heng et al. [24], through the use of the AR model over the energy range from 100 to 50 keV and their results are in good agreement when compared with those obtained by experiments wherever available. Blanco and García reported TCS and elastic ICS for electron scattering from benzene, calculated via the IAM—screening corrected additivity rule (IAM-SCAR) approach [25]. Absolute cross sections for elastic electron collisions with benzene measured in the 100–1000 eV range and calculations performed according to the IAM model were reported by Iga et al. [26]. Also using the IAM model, Er-Jun et al. calculated elastic DCS in the energy range 100–1000 eV [27]. Experimental differential, integral, and momentum transfer cross sections for elastic electron scattering by benzene were measured by Sanches and coworkers [28] for energies from 50 to 1 keV. The comparison of these results with existing theoretical data shows significant discrepancies, particularly at incident energies below 200 eV. IAM-SCAR calculations, for elastic scattering, were carried out by Kato et al. [29] and compared to then available results. Measurements of DCS and ICS of the unresolved 1^1B_{1u} and 1^3E_{2g} electronic states and the 1^1E_{1u} electronic state of benzene were reported by Kato et al. [30], for angles between 3° and 130° and in the energy from 10 to 200 eV. More recently, by using a theoretical method based on the single-center-expansion close-coupling framework and corrected by the Padé approximant, de Souza et al. [31] reported on elastic differential, integral, and momentum transfer as well as inelastic and total (elastic + inelastic) cross sections for impact energies ranging from 20 to 500 eV. Singh et al. employed a multi-scattering center spherical complex optical potential method to calculate TCS and total ionization cross sections (TICS) for benzene and other benzene derivatives [32]. In their study, Barbosa et al. [33] revisited the problem with the use of the SMC method and discussed the presence of shape resonances, a virtual state, and a Ramsauer–Townsend minimum in the low-energy regime. Comparison of their calculated ICS and DCS with the available data from the literature suggested improvement in the agreement between theory and experiment. Also, electronic excitation, momentum transfer, ionization, and total collision cross sections, along with the differential elastic cross sections were computed for low energies (0.01-20 eV) by Prajapati et al. [34] using the R-matrix method. Allan and collaborators [35] and Costa and collaborators [36] both performed joint experimental–theoretical investigations on electron scattering from benzene and have reported on elastic DCS at the scattering angles of 90° and 135°, and TCS and elastic ICS, respectively. Finally, Lozano et al. [37] have reported double and triple differential cross sections for electron impact ionization of benzene.

Taken together, these studies shed light on several important aspects relating to the problem of electron scattering by the benzene molecule. However, among some drawbacks and puzzling issues that still remain, the scarcity of studies concerning the electronic excitation of benzene by electron impact should be highlighted. One of the challenges to be addressed in the treatment of electronically inelastic collisions, at least from the theoretical perspective, is related to the con-

vergence of the multichannel coupling with respect to the number of channels. Proper handling of this aspect, in turn, involves not only an accurate description of a number of excited states but, perhaps more importantly, a judicious choice on how many and which channels (energetically accessible states to the molecular target) should be included in the scattering calculations.

In the present investigation, we report on elastic and electronically inelastic scattering of electrons by benzene using the SMC method [38,39]. DCS and ICS for elastic scattering and for excitation of bands I, II, and III (for which there are no experimental results available), and also for bands IV and V (a single experimental study [30]), are reported for the energy range 10–50 eV. Our full set of cross sections is provided in the Zenodo repository, at http://doi.org/10.5281/zenodo.5567092.

In order to account for the high computational cost in getting reliable results for polyatomic targets, we employed the parallel version [40] of the SMC codes in an implementation that makes use of norm-conserving pseudopotentials (SMCPP) [41] and single-excitation configuration interaction techniques for the target description [42]. In addition, we make use of a procedure that allows for many more open channels to be accounted for in the calculations [43]. It is the purpose of this work: (i) to address the need for reliable cross sections for electronic excitation by electron impact and (ii) to investigate how the presence of substantially more open channels (in particular, in order to evaluate the influence of Rydberg states) impacts on the quality of the DCS for elastic and electronically inelastic scattering of low-energy electrons by benzene. To the best of our knowledge, there are no previous calculations for the electronic excitation of these bands reported in the literature.

The remainder of this paper is organized as follows. In the next section, the SMC method is briefly summarized and the computational aspects of our calculations are described. The results are presented and discussed in Sect. 3 and, finally, some concluding remarks are outlined in Sect. 4.

2 Theory and computational aspects

The SMC method is an ab-initio approach proposed by Takatsuka and McKoy [38,39] to simulate the electron–molecule collision, which is based on a variational formulation to the scattering amplitude. The method can be applied to molecules of arbitrary geometry and accounts for: (i) the scattering wave function antisymmetrization, (ii) the polarization of the molecular electronic cloud, (iii) the competition of the flux probability among all energetically accessible electronic states of the system (multichannel coupling), and (iv) Bachelet, Hamann, and Schlüter (BHS) pseudopotentials [44] to describe the nuclei and core electrons [41]. The theory and computational aspects of the SMC method have been reviewed by da Costa et al. [45], and as such here we only summarize the key aspects of the present application.

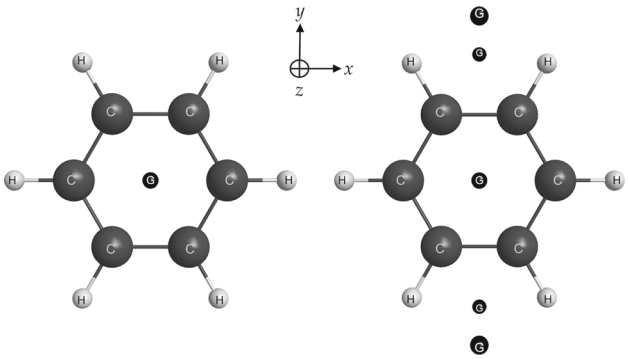

Fig. 1 Schematic illustration to represent the position of the extra centers used in the composition of the basis sets B1 (left) and B2 (right). The figures were generated with the software MacMolPlt [49]

The ground state geometry of benzene was optimized within the GAMESS-US package [46], using the second-order Møller-Plesset perturbation theory (MP2) and the aug-cc-pVDZ basis set. With the same package, we also carried out Hartree–Fock self-consistent field calculations to obtain the electronic ground state. All calculations have been performed within the D_{2h} point group. In our first round of scattering calculations, we employed the $5s5p3d$ basis set for the carbon atoms (the same as used by Bettega [47]), the $4s/3s$ Dunning basis set for the hydrogen atoms [48] supplemented with one p function with exponent 0.75 a_0^{-2}, and an additional $3s3p2d$ set of diffuse functions placed at the center of mass. This defines our basis set B1, which is flexible enough to describe the lower-lying Rydberg states. In order to explore the role of the higher-lying Rydberg states in the multichannel coupling, we have additionally performed a second round of scattering calculations, for a larger basis set B2. It comprises all functions from the B1 set plus $3s3p$ diffuse exponents placed at the vertices $(0, \pm 5, \pm 3)$ a_0 of a rectangle centered at the origin. Figure 1 illustrates the molecular orientation and the positions of the extra centers, while Table 1 shows the exponents of the Gaussian functions placed at the center of mass and at the extra centers. These exponents were obtained from the last exponents of the $5s5p3d$ basis set, by recursive divisions by four.

In the target description and scattering calculations, we employed improved virtual orbitals (IVOs) [50] from the lowest non-degenerate a_g occupied orbital and triplet multiplicity. The excited states were described at the truncated configuration interaction singles (TCIS) approach, where a subset of all single excitation is selected based on an energy cutoff $\varepsilon_{\text{open}}$, as described elsewhere [43]. Here, we emphasize that the IVO calculations served only to provide a more suitable set of orbitals than the canonical virtual orbitals, whereas in the scattering calculations the excited states were described with the TCIS approach. The key idea behind the TCIS technique is to select the single excitations

Table 1 Exponents of the Gaussian functions placed at the center of mass and at the extra centers (in units of a_0^{-2}). The coefficient of each Gaussian function is 1.0

Type	Exponent
s	0.009995
s	0.002499
s	0.000625
p	0.018063
p	0.004516
p	0.001129
d	0.025279
d	0.006320

that are most important to describe the excited states lying below $\varepsilon_{\text{open}}$, while trying to recover the full configuration interaction singles (FCIS) results as much as possible. Here, we employed $\varepsilon_{\text{open}} = 10$ eV, which gave rise to 116 excited states for the B1 basis set, and 304 excited states for the B2 basis set (lying below 10.02 eV in the latter). All these states were considered as open channels in our calculations, and together with the elastic channel, we have a total of 117 and 305 channels, for basis sets B1 and B2, respectively. This means that all 117/305 states are simultaneously competing in the multichannel coupling scheme. From here on, we refer to these two levels of calculations as 117CH-B1 and 305CH-B2. The scattering wave function was expanded in a set of configuration state functions, which are spin-adapted antisymmetrized products of all single excitations contained in the TCIS description and the set of all IVOs.

The momentum space integrals that appear in the projected Green's function were computed numerically. More details about this aspect of the calculations are given in Ref. [45]. Both off-energy-shell and on-energy-shell terms were computed with a Gauss–Legendre quadrature, in angular and radial components of the linear momentum vector. In addition, the radial integral was divided into two intervals, from 0 to $k_{\max}$ (integration in the variable k) and from $k_{\max}$ to infinity (integration in the variable k^{-1}), with $k_{\max} = 1.6a_0^{-1}$. To ensure the quality of the numerical procedures, we performed a convergence analysis by comparing the magnitudes and shapes of the computed DCS. Convergence has been achieved with 26 radial points in each radial interval. Spherical coordinates were employed for the angular integration, with the same number of quadrature points for both polar and azimuthal angles. We settled with 26 quadrature points in each coordinate for the off-energy-shell terms, and with 16 points for the on-energy-shell terms.

With the goal of identifying how many and which excited states would compose the two bands for which electronic excitation DCS are available [30], we calculated vertical excitation energies with the equation-of-motion (EOM) coupled cluster (EOM-CC) with singles and doubles (EOM-CCSD) [51], and with the iterative approximate coupled cluster CC3 (EOM-CC3) [52,53] levels of theory. To do these calculations, we used the PSI4 [54] and CFOUR [55,56] quantum chemistry packages. We employed the aug-cc-pVDZ basis set for the hydrogen atoms and the d-aug-cc-pVDZ basis set for the carbon atoms. The doubly augmented diffuse functions were found to be important to describe some of the lower-lying Rydberg states. Core orbitals were kept frozen. The transition dipole moments obtained at the EOM-CCSD calculations were also employed to perform the Born-closure procedure [57], which aims at correcting for the poor description of long-range interactions in the SMC method.

3 Results and discussion

3.1 Elastic channel

The available elastic DCS are shown in Fig. 2, according to ours and previous calculations [12,14,31,33,34] and to the available experimental data [16,28,29]. We found that accounting for higher lying Rydberg states (when going from the 117CH-B1 to the 305CH-B2 results) produces only marginal effects on the shapes and magnitudes of the elastic DCS. Our results are in quite good agreement with the available experimental data at 15, 20, and 30 eV. Importantly, our results are much closer to experiment than the previous calculations, which employed the single-center-expansion method with model potentials [12], the independent atom model [28], the SMC method with one open channel [14,33], and the spherical complex optical potential method [34]. The inclusion of more open channels compared to the aforementioned calculations improves the agreement with the experiment, which is consistent with many previous studies with the SMC method for other molecular targets [43,58–67].

At 40 and 50 eV, however, the magnitudes of the DCS still appear somewhat overestimated in our calculations for intermediate angles. This probably reflects the lack of higher-lying discrete excited states, but also continuum states (ionization channels), that are not currently implemented in the SMC method. At 10 eV, the overall comparison is less clear, as our computed DCS lie mostly below the experimental ones for electron scattering angles above about 40°, and does not significantly improve with respect to the previous theoretical results. The origin of this discrepancy is unclear. It might be that the description of polarization effects still has room for improvement, which would affect particularly the cross sections computed at the lower impact energies. We also notice that a similar disagreement has been recently observed for ethanol [43], where the calculations also employed the SMC method and comparable methodological procedures as in the present study.

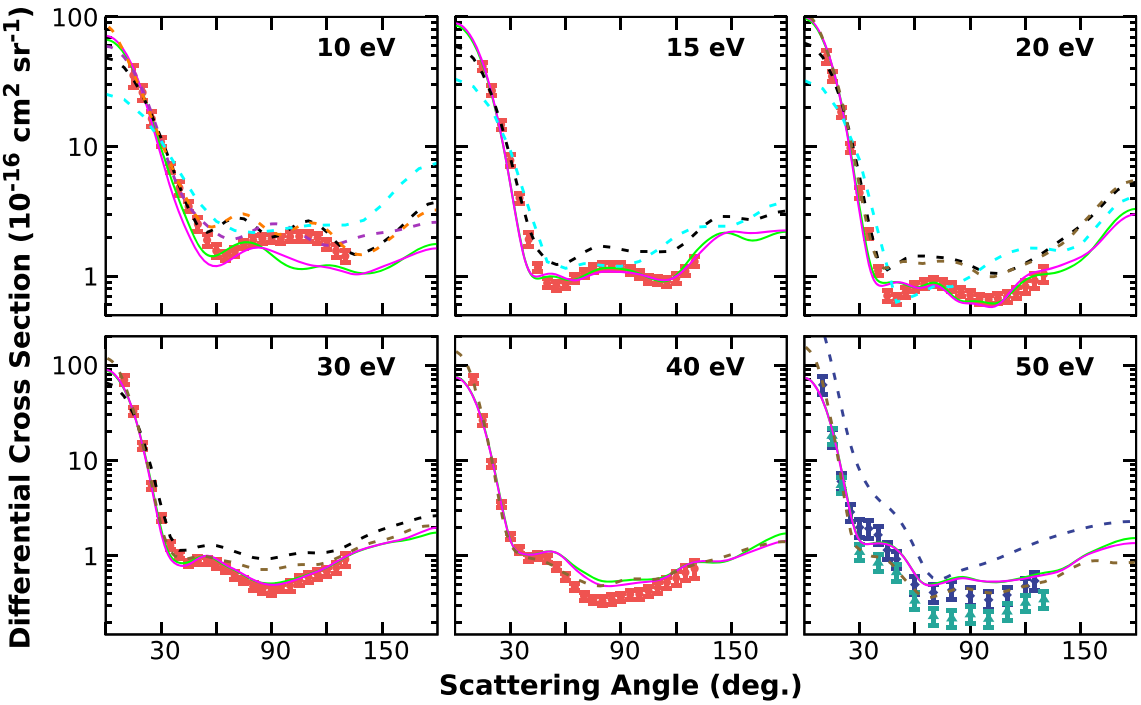

Fig. 2 Elastic differential cross sections for electron scattering from benzene. The full lines are the present results for the 117CH-B1 (green) and 305CH-B2 (magenta) calculations. The dashed lines correspond to the previous calculations, reported by Bettega et al. [14] (black), Barbosa et al. [33] (purple), Gianturco et al. [12] (orange), Prajapati et al. [34] (cyan), de Souza et al. [31] (brown), and Sanches et al. [28] (blue). Experimental data from Cho et al. [16] (light red dots), from Sanches et al. [28] (blue diamonds), and from Kato et al. (green triangles) [29] are also shown

3.2 Characterization of the electron energy loss spectra

Let us now discuss the characterization of the electron energy loss spectra of Kato et al. [30], from which DCS of bands IV and V have been obtained. Our goal here is to identify how many and which states compose these bands, and for that we did EOM-CCSD and EOM-CC3 calculations. A detailed discussion about the character of these excitations goes beyond the scope of this paper. Similarly, a detailed discussion and comparison concerning the lower-lying excited states can be found in Ref. [68] and references therein. Table 2 shows the vertical excitation energies obtained at the EOM-CC3, EOM-CCSD, FCIS, and TCIS levels of theory, for both singlet and triplet excited states, as well as the experimental results taken from Refs. [5,7,8,69,70]. Since the extra centers of basis set B2 do not transform according to all the symmetries of the D_{6h} point group (only for those of the D_{2h} subgroup), there is an artificial energy splitting for the physically degenerate states of E_{1g}, E_{2g}, E_{1u}, and E_{2u} symmetries. This effect is rather small though (maximum of 0.02 eV), and as such only the average energies of these states are shown in Table 2. In addition, Fig. 3 shows a schematic comparison between the EOM-CC3 vertical excitation energies and the specific EELS spectra shown in the study of Kato et al. [30]. Our EOM results support three states in band IV and eighteen states in band V (in some sense somewhat arbitrarily defined as the 6.6 eV −7.6 eV energy range). Importantly, while the CIS calculations are less accurate than the EOM-CC, they still seem to provide a qualitatively correct description of the excited states surveyed here. We recall that in the scattering calculations the excited states are described with the TCIS approach, as explained in the previous section.

In Ref. [30], the electronic excitation DCS were obtained by deconvoluting the EELS spectra. This can be challenging and to a certain degree also arbitrary, whenever there are wide and overlapping bands, which is the case of band V in benzene. In this sense, the experiments actually provide the DCS of the whole band, rather than DCS of an individual excited state, and therefore, a proper comparison to theory is not simple. On the one hand, we should know which and how many excited states belong to a given band, which might require an accurate level of description. On the other hand, the deconvolution itself brings some uncertainty to the comparison, as it is not obvious how to account for states that are in the frontier of the band. Kato et al. [30] have reported DCS for bands IV and V of benzene. The comparison for the former is straightforward, since the two singlets and one triplet of this band are well separated from lower- and higher-lying states. The situation is more tricky for band V, where

Table 2 Vertical excitation energies (in eV) of singlet and triplet excited states of benzene, according to experiment and to different EOM and CIS calculations (for the geometry optimized at the MP2/aug-cc-pVDZ level of theory)

Band	State	Exp.[a]	EOM-CCSD	EOM-CC3	FCIS[b]	FCIS [c]	TCIS[b]	TCIS[c]
I	1^3B_{1u}	3.95	3.87	4.05	3.13	3.13	4.15	4.14
II	1^3E_{1u}	4.76	4.82	4.76	4.71	4.71	4.84	4.84
III	1^3B_{2u}	5.60	5.71	5.75	5.33	5.33	5.54	5.53
IV	1^3E_{1g}		6.34	6.32	6.37	6.37	6.50	6.50
V	1^3A_{2u}		6.85	6.84	6.77	6.77	6.97	6.96
	1^3E_{2u}		6.97	6.95	7.04	7.03	7.12	7.11
	1^3A_{1u}		7.09	7.06	7.25	7.24	7.26	7.25
	2^3E_{1u}		7.11	7.11	7.07	7.05	7.14	7.12
	2^3E_{1g}		7.42	7.38	7.38	7.37	7.49	7.47
	1^3B_{1g}		7.54	7.54	7.60	7.58	7.67	7.67
	1^3B_{2g}		7.56	7.51	7.64	7.62	7.65	7.64
	1^3E_{2g}		7.56	7.34	7.33	7.33	7.77	7.75
	3^3E_{1g}		7.58	7.54	7.64	7.63	7.68	7.67
II	1^1B_{2u}	4.90	5.07	4.97	5.87	5.86	6.00	5.99
IV	1^1B_{1u}	6.20	6.44	6.38	6.03	6.02	6.75	6.71
	1^1E_{1g}	6.33	6.39	6.36	6.48	6.48	6.57	6.57
V	1^1A_{2u}	6.93	6.91	6.91	6.89	6.88	7.04	7.03
	1^1E_{1u}	6.94	7.08	7.01	7.14	7.12	7.18	7.16
	1^1E_{2u}	6.95	6.99	6.97	7.07	7.06	7.13	7.12
	1^1A_{1u}		7.08	7.05	7.25	7.24	7.26	7.25
	2^1E_{1u}	7.41	7.38	7.26	7.85	7.78	8.09	8.07
	2^1E_{1g}		7.47	7.46	7.50	7.48	7.56	7.55
	1^1B_{2g}		7.56	7.56	7.64	7.62	7.67	7.66
	1^1B_{1g}		7.57	7.54	7.65	7.63	7.68	7.66
	3^1E_{1g}		7.58	7.56	7.67	7.66	7.70	7.69

[a] Refs. [5,7,8,69,70]
[b] 117CH-B1 calculation
[c] 305CH-B2 calculation

many close-lying states appear in its higher energy limit. Here, the reported DCS for band V comprise the summed contribution from all states between 6.6 eV and 7.6 eV (as obtained in the EOM-CC3 calculation). We also tested how including fewer of more states would affect the results, and we have seen only minor changes in the magnitudes (by 5% when discarding the two uppermost states from the band).

3.3 Electronic excitation channels

The electronic excitation DCS for bands I, II, and III are shown in Figs. 4, 5, and 6. These results were obtained by summing the contribution of the states belonging to each band, according to our characterization presented in Table 2. For these bands, we are not aware of existing experimental or theoretical results to compare with. The DCS are similar in both 117CH-B1 and 305CH-B2 levels of calculation; however, the latter provides overall smaller magnitudes. The shape of the DCS is mostly preserved in both calculations; however, some more pronounced differences can be seen at lower energies.

The electronic excitation DCS for band IV are shown in Fig. 7. According to our excited state calculations, this band has contributions from 1^1B_{1u}, 1^3E_{1g}, and

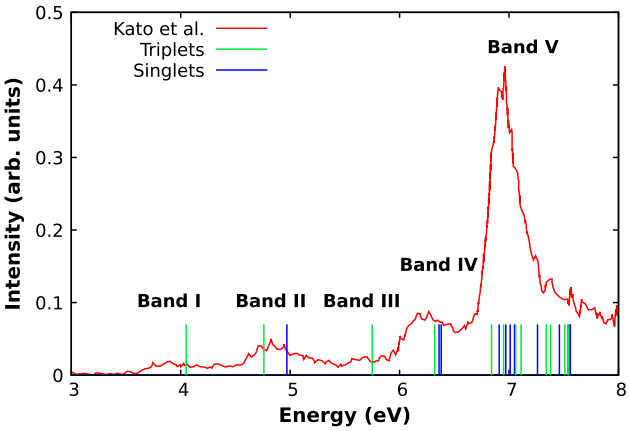

Fig. 3 Comparison between the typical EELS spectra presented in Ref. [30] (measured at the impact energy of 15 eV and the scattering angle of 50°) and the vertical excitation energies computed at the EOM-CC3 level of theory. The heights of the bars are arbitrary, for ease of viewing

1^1E_{1g} states. Our assignment is in line with other calculations (see Ref. [71] and references therein), and differs from the one of Kato et al. [30], who suggested only 1^1B_{1u} and 1^3E_{2g} states. As for the previous bands,

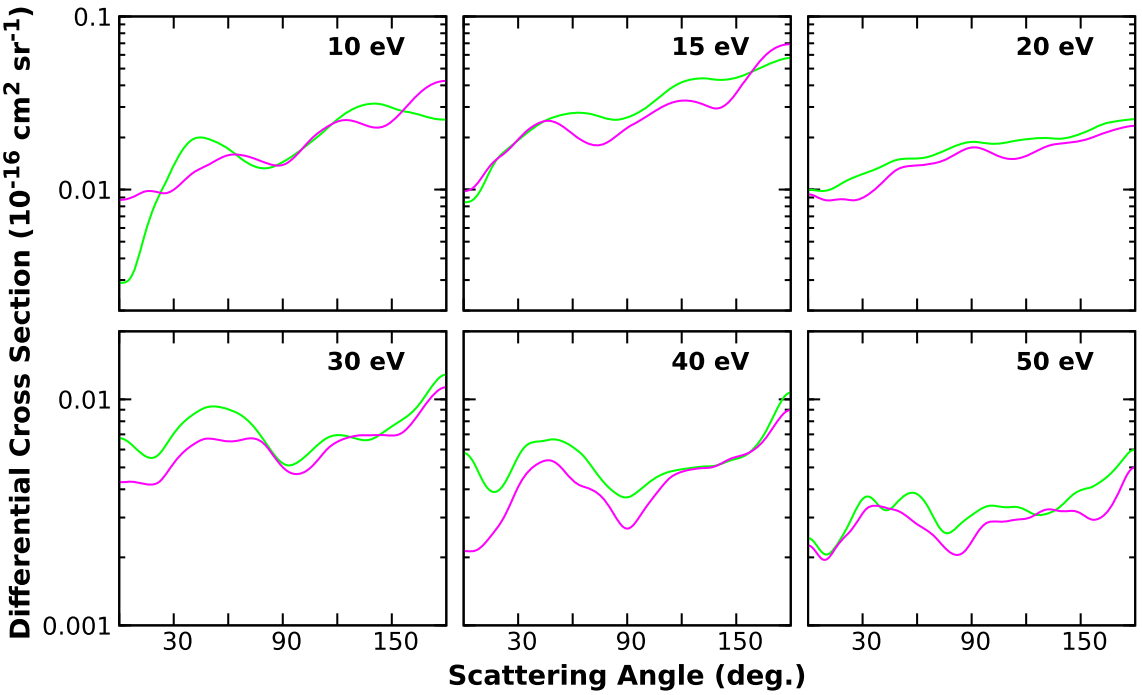

Fig. 4 Electronic excitation differential cross sections for band I of benzene, according to our 117CH-B1 (green) and 305CH-B2 (magenta) calculations

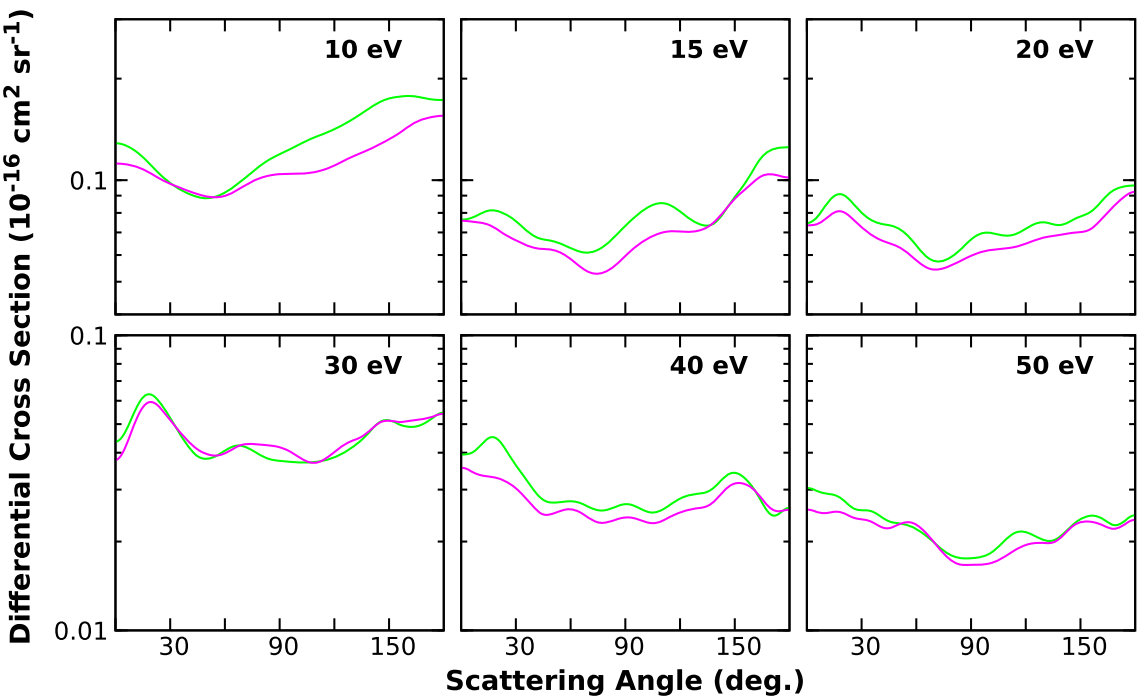

Fig. 5 Electronic excitation differential cross sections for band II of benzene, according to our 117CH-B1 (green) and 305CH-B2 (magenta) calculations

we found smaller magnitudes in the 305CH-B2 than in the 117CH-B1 calculation. Counting on the available experimental data for this band [30], here we see the relevance of accounting for higher-lying Rydberg states to the excitation cross sections, specially at lower collision energies. This effect tends to diminish with increasing impact energies, though it remains non-negligible (recall the logarithmic scale). At intermediate and larger angles, the 305CH-B2 DCS are in good agreement with the experimental data at 10 and

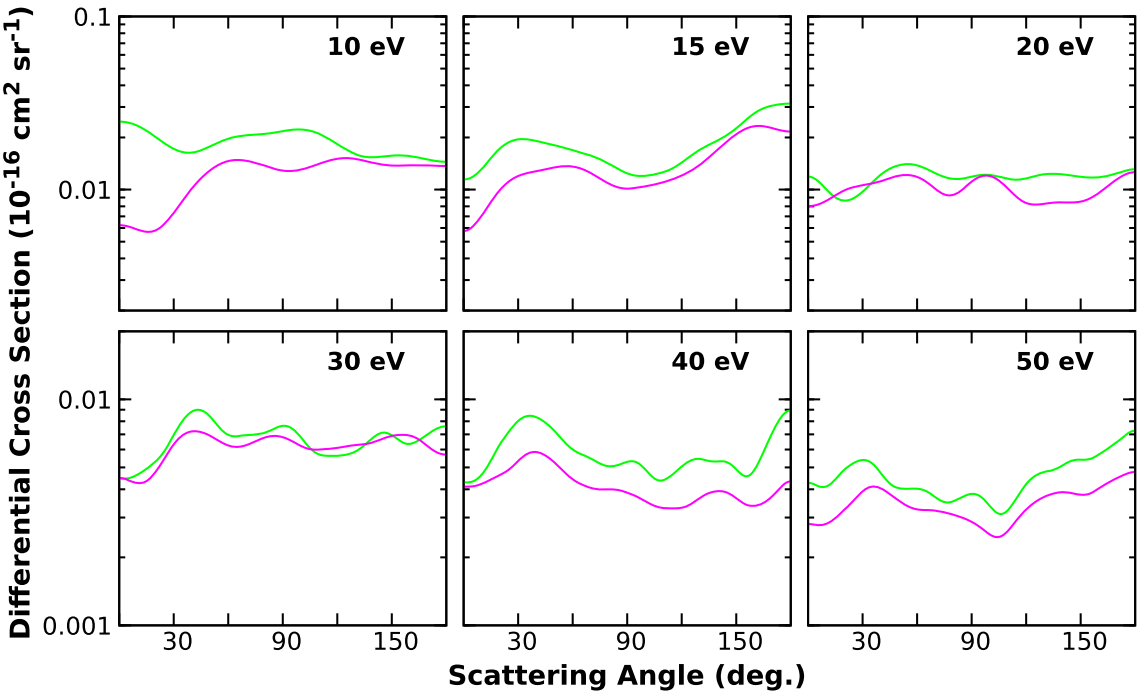

Fig. 6 Electronic excitation differential cross sections for band III of benzene, according to our 117CH-B1 (green) and 305CH-B2 (magenta) calculations

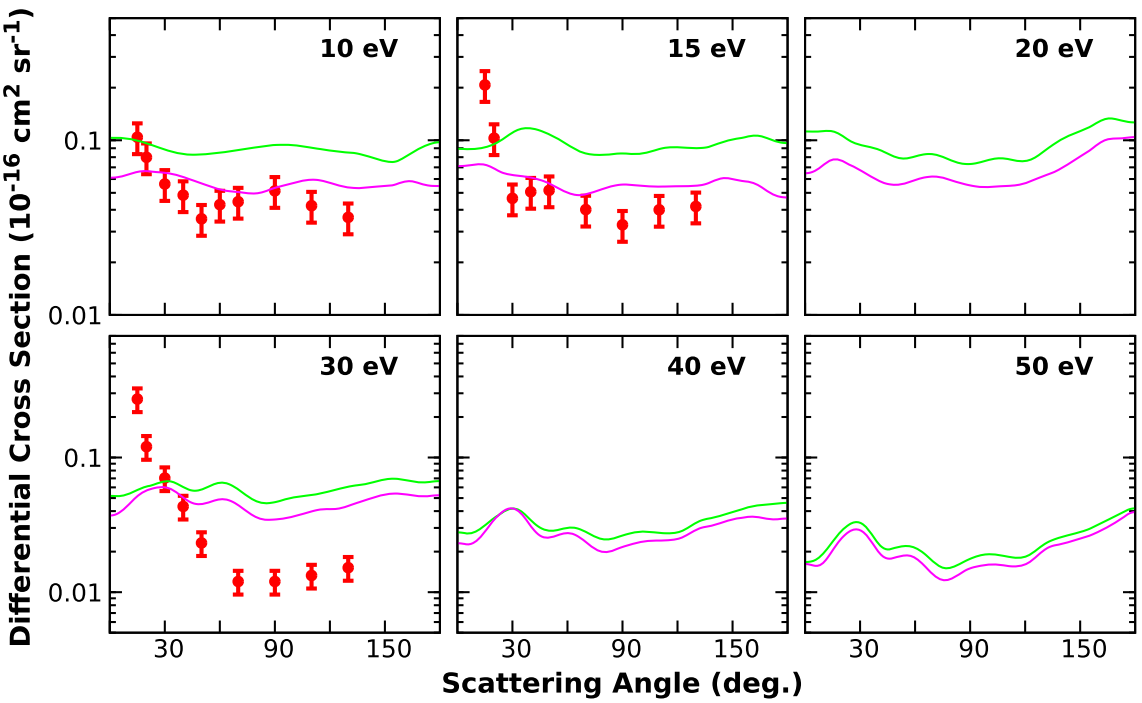

Fig. 7 Electronic excitation differential cross sections for band IV of benzene, according to our 117CH-B1 (green) and 305CH-B2 (magenta) calculations. Also shown are the experimental results (red dots) reported by Kato et al. [30]

15 eV. At 30 eV, however, the calculations overestimate the experimental DCS, a sign that higher-lying excited states, missing in our calculations, should be included in the multichannel coupling scheme.

The poor agreement at smaller angles could be related to the use of square-integrable functions as basis sets to describe long-range interactions. However, all states in this band are dipole forbidden, and therefore, electronic excitation is expected to take place via short-range interactions (at least in the equilibrium geometry), in principle well described in the SMC method. In turn, the forward peaking observed experi-

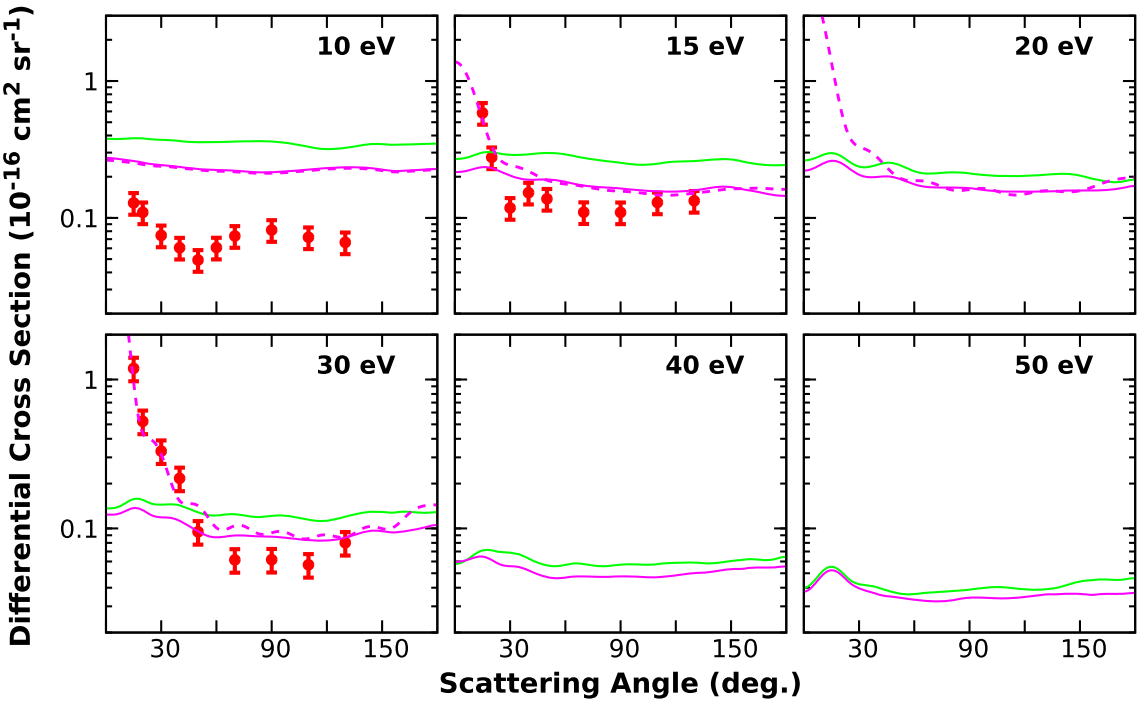

Fig. 8 Electronic excitation differential cross sections for band V of benzene, according to our 117CH-B1 (green) and 305CH-B2 calculations (magenta full lines), and 305CH-B2 using the Born-closure procedure (magenta dashed lines). Also shown are the experimental results (red dots) reported by Kato et al. [30]

mentally hints at long-range dipole-allowed excitation, which could take place at distorted geometries. This might suggest significant vibronic effects in the excitation of benzene by electron impact.

Figure 8 displays the DCS for band V. Our calculations point out to many more excited states in this band than the single 1^3E_{1u} state suggested by Kato et al. [30]. The DCS of this state alone lie around one order of magnitude below the sum of all states present in the band (not shown), which demonstrate the need for an accurate characterization of the bands. Most of the findings concerning this band are similar to those discussed for band IV. In this case, however, the agreement with experiment at intermediate angles is less satisfying at 10 eV, but more so at 30 eV. The origin of this different behavior for bands IV and V is unclear. In contrast to the previous bands, this one presents dipole-allowed excitations, for which we employed the Born-closure procedure. The EOM-CCSD oscillator strengths of the dipole-allowed transitions are 0.113 (1^1A_{2u}), 0.311 (1^1E_{1u}), and 0.424 (2^1E_{1u}). The cutoff angular momenta were set to $\ell = 5$ for 15 eV and $\ell = 7$ for 10 eV, 20 eV, and 30 eV, which was chosen such that the Born correction does not significantly affect the DCS at intermediate and larger angles. The Born closure affects mostly the smaller angles and becomes more relevant at higher energies, having virtually no effect at 10 eV, and reproducing the forward peaking at 30 eV. We have not performed such a procedure for 40 and 50 eV, however, due to numerical instabilities encountered at these energies.

3.4 Integral cross sections

The left panel of Fig. 9 compares our computed elastic ICS with previous calculations [12,14,29,31,33] and available experimental data [16,28,29]. In the whole 10–50 eV range, our results fall within the error bars of the measurements of Cho et al. [16] and Sanches et al. [28], whereas the data from Kato et al. [29] lie somewhat underestimated with respect to ours and previous reports. Meanwhile, the magnitudes of our elastic ICS are lower than in most of the previous calculations [12,14,31,33], being overall closer to the IAM-SCAR calculations of Kato *et al.* [29].

The ICS for electronic excitation of bands I–V are shown in the right panel of Fig. 9. The magnitudes for excitation of bands I and III are quite small, as each band presents one triplet state only. Singlet states appear in bands II and IV, which in turn have larger cross sections. Band V is the most prominent one, having three pronounced dipole-allowed transitions, and many other excited states with relevant contributions. The comparison with respect to the experimental electronic excitation ICS [30] would seem quite encouraging (except for band V at 10 eV). However, the DCS (see Figs. 7 and 8) reveal that the apparent good agreement is often due to a cancellation of errors in the smaller and intermediate scattering angles. As for the DCS, the Born-closure procedure has a huge impact on the ICS, specially at higher energies. This last result suggests that adopting the same correction to excitations of the higher lying states (beyond band V) might also be critical for obtaining more accurate electronic excitation

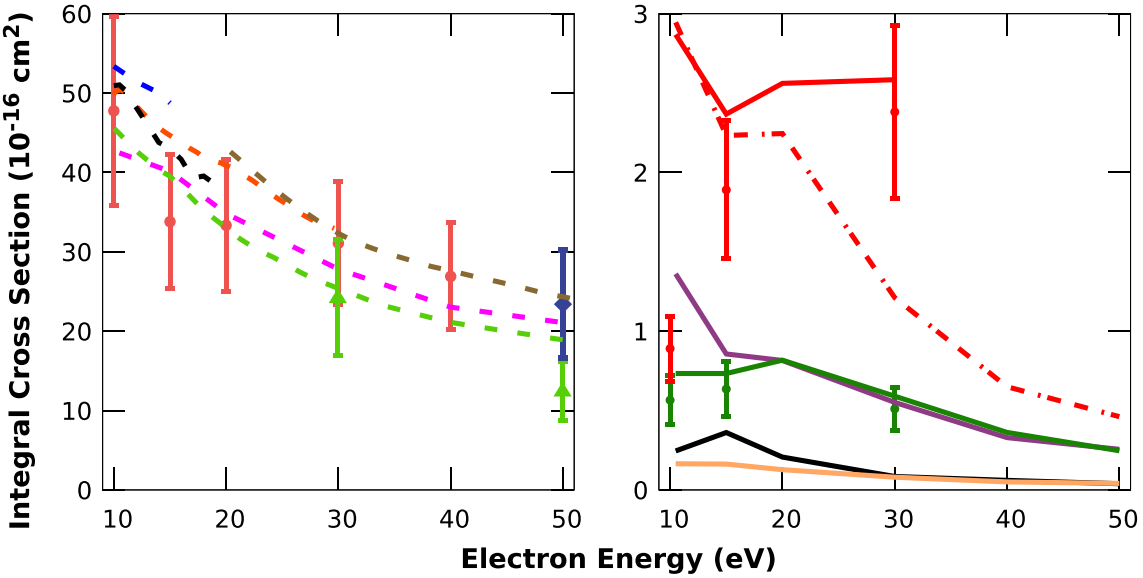

Fig. 9 Integral elastic (left panel) and electronic excitation (right panel) cross sections for electron impact on benzene. In the left, results from our 305CH-B2 calculations (magenta), according to previous calculations (dashed lines) by Gianturco et al. (orange) [12], Bettega et al. (black) [14], Kato et al. (green) [29], de Souza et al. (brown) [31], and Barbosa et al. (blue) [33], and to measurements (marks) by Cho et al. (light red dots) [16], Sanches et al. (blue diamonds) [28], and Kato et al. (green triangles) [29]. In the right, results from our 305CH-B2 calculations for excitation of bands I (black), II (purple), III (orange), IV (dark green), and V, the last one without (dashed-dotted red) and with the Born-closure correction (solid red), as well as the experimental results [30] for bands IV (dark green dots) and V (red dots)

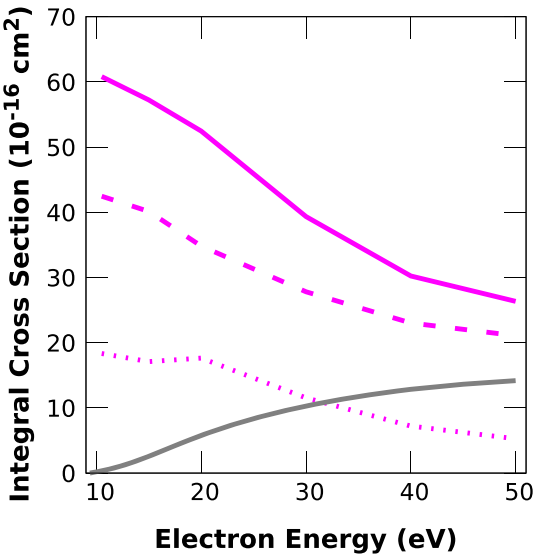

Fig. 10 Cross sections for electron impact on benzene, according to our 305CH-B2 calculations (magenta): TCS (solid line), elastic ICS (dashed line), and electronic excitation ICS (dotted line). The BEB TICS from Ref. [74] (solid gray) are also shown

ICS as well as TCS. That would require the transition dipole moments calculated at the TCIS level of theory, which is not currently available in our computational codes. Such an implementation is planned for the future.

The ICS for the elastic and the sum of all electronic excitation channels are shown in Fig. 10, together with their sum, which represent the TCS in our 305CH-B2 calculations. The Binary–Encounter–Bethe (BEB) [72,73] TICS (from Ref. [74]) are also shown, since the ionization channels are currently lacking in the SMC method. This figure provides an integrated view of the relative contributions of elastic, electronic excitation, and ionization channels to the total cross sections. We further notice that the five lower-lying bands we have focused on make up for a rather small part of the sum of all electronic excitation channels (compare Figs. 9 and 10). Bands I to V account for a factor of 0.3 of the summed excitation cross sections at 10 eV, decreasing to 0.2 at 50 eV.

3.5 Total cross sections

The comparison between our 117CH-B1 and 305CH-B2 calculated TCS and previous theoretical [12,15,20,31,32,34,36] and experimental [11,21,36,75] results are presented in Fig. 11. The difference between our two levels of calculations is quite small, showing that inclusion of higher-lying Rydberg states in the multichannel calculations is not really important for this particular purpose. Between 10 and 25 eV, our results compare very favorably in shape and magnitude with the most recent experimental results [11,21,36]. However, the comparison degrades at higher energies, as our TCS drop more steeply than most of the previous reports. It is also worth mentioning the wide variation of the calculated TCS among different methodologies. We further present our results with the further contribution of the

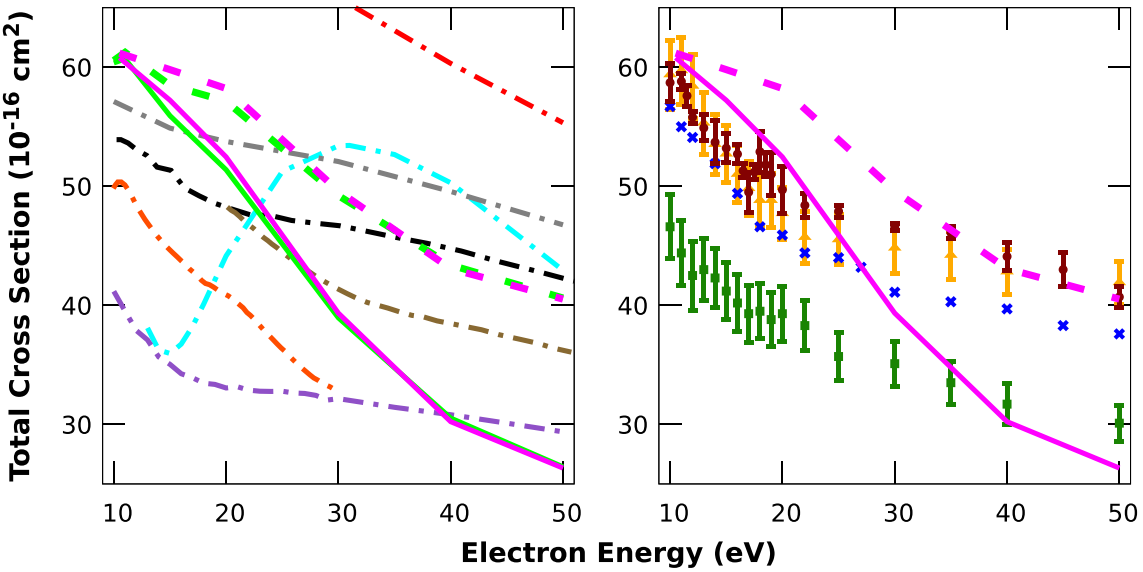

Fig. 11 Total cross sections for electron impact on benzene. Results for the sum of our integral elastic and electronic excitation cross sections from our 117CH-B1 (green) and 305CH-B2 (magenta) calculations, are shown in full lines, and further with addition of TICS computed with the BEB method [74] are shown as dashed lines. In the left panel, the dashed-dotted lines correspond to the calculations from Gianturco et al. (orange) [12], Jiang et al. (red) [15], de Souza et al. (brown) [31], Costa et al. (gray) [36], Sun et al. (black) [20], Singh et al. (purple) [32], and Prajapati et al. (cyan) [34]. In the right panel, experimental data from Sueoka (green squares) [75], Mozejko et al. (blue crosses) [11], Makochekanwa et al. (yellow triangles) [21], and Costa et al. (dark red color dots) [36] are plotted and compared with our 305CH-B2 results, both without (full lines) and with (dashed lines) the BEB TICS added in

BEB TICS (from Ref. [74]), as a simple attempt to correct for the lack of ionization channels in our calculations. This improves the comparison to experiment at the higher energies, at the cost of worsening the agreement at the lower energies, suggesting that the diffuse discrete states would be mimicking in some way the ionization continuum. This possibility will be explored in future studies. Likewise, more open electronic excitation channels would be needed, due to the high density of states at higher energies. We further notice that our computed elastic ICS (see Fig. 10) compare more favorably to experiment than our TCS, suggesting that the discrepancies found would likely arise from the description of inelastic channels. As mentioned previously, we have not performed a Born-closure correction for excitation of states lying beyond band V, which might have a non-negligible impact on the TCS.

4 Conclusion

We have presented a theoretical study on low energy electron impact excitation of benzene, based on scattering calculations with the Schwinger multichannel method. Total cross sections, differential and integral cross sections for the elastic channel and for excitation of the first five bands have been presented, and our results have been compared to previous experiments and calculations, when available. To the best of our knowledge, we report the first set of ab-initio calculations of electronic excitation DCS for benzene.

Our computed elastic DCS compare very favorably with the experimental data, showing better overall agreement than in previously reported calculations. In turn, the DCS for electronic excitation are much smaller than their elastic counterpart, making their theoretical description more difficult. Yet, our calculations provided the correct order of magnitudes at intermediate scattering angles. With the help of the Born-closure procedure, the peak at small angles experimentally observed for band V is correctly reproduced as well. In contrast, a similar forward peaking behavior has been detected for band IV, and the lack of dipole-allowed transitions in this energy range suggests important vibronic effects. The same conclusions hold for the elastic and electronic excitation ICS. We paid special attention to the characterization of the bands measured in electron energy loss spectroscopy, from which experimental DCS are obtained. Not accounting for the correct states that compose each band can lead to significant errors in the comparison.

The computed TCS also presented a good agreement with measurements at lower energies; however, they dropped too fast toward higher energies. Summing the BEB TICS ameliorates the comparison to some extent. The poorer agreement at higher energies might be related to lack of even higher excited states (ionization continuum included), or else to a deficient description of the electronic excitation mediated by the long-range interaction. These aspects will be further investigated in the future.

One of our main goals was to assess the influence of including higher-lying Rydberg states in the multi-

channel coupling scheme, which motivated our two sets (117CH-B1 and 305CH-B2) of scattering calculations. We found a rather small effect on the elastic DCS and ICS, a general reduction of the DCS and ICS for electronic excitation of the lower-lying bands, and again a modest effect on the TCS. In addition, the differences between the two calculations often declined with increasing energy. Therefore, accounting for such states might or might not be recommended (from a practical point of view) depending on the particular goals of a given study. While some degree of convergence with respect to the number of open channels can be alluded to, most notably in the elastic channel, we recall that the key difference between the two multichannel calculations lie on the number of Rydberg states. As such, the influence of even higher-lying Rydberg states is likely minor.

Finally, we performed EOM-CCSD and EOM-CC3 calculations for all states extending up to around 7.6 eV, covering a total of 12 singlet and 13 triplet excited states. The computed vertical excitation energies may serve as reference values for future calculations.

Acknowledgements A.G.F. acknowledges support from Coordenaão de Aperfeiçoamento de Pessoal de Nível Superior—Brasil (CAPES) —Finance Code 001, and M.A.P.L. and R.F.C. acknowledge the Brazilian agency Conselho Nacional de Desenvolvimento Científico e Tecnológico (CNPq). This research used the computing resources and assistance of the John David Rogers Computing Center (CCJDR) in the Institute of Physics "Gleb Wataghin," University of Campinas. M.J.B. acknowledges funding from the Australian Research Council through Grant # DP180101655.

Author contributions

AGF performed the calculations. All authors analyzed and discussed the results and contributed to the outline of the manuscript. AGF, RFC, and FK wrote the first version of the manuscript. MJB and MAPL contributed to the final version of the manuscript.

Data Availability Statement This manuscript has associated data in a data repository. [Authors' comment: Our full set of cross sections is provided in the Zenodo repository, at http://doi.org/10.5281/zenodo.5567092].

References

1. Z. Ates-Alagoz, N. Coleman, M. Martin, A. Wan, A. Adejare, Chem. Biol. Drug. Des. **80**, 853 (2012)
2. E. Alizadeh, T.M. Orlando, L. Sanche, Annu. Rev. Phys. Chem. **66**, 379 (2015)
3. J.D. Gorfinkiel, S. Ptasinska, J. Phys. B: At. Mol. Opt. Phys. **50**, 182001 (2017)
4. F.H. Read, G.L. Whiterod, Proc. Phys. Soc. **85**, 71 (1965)
5. E.N. Lassettre, A. Skerbele, M. Dillon, K. Ross, J. Chem. Phys. **48**, 5066 (1968)
6. R.N. Compton, R.H. Huebner, P.W. Reinhardt, L.G. Christophorou, J. Chem. Phys. **48**, 901 (1968)
7. J.P. Doering, J. Chem. Phys. **51**, 2866 (1969)
8. J.P. Doering, J. Chem. Phys. **67**, 4065 (1977)
9. D. Mathur, J.B. Hasted, J. Phys. B: Atom. Mol. Phys. **9**, L31 (1976)
10. J.S. Mahant Shetty, S.M. Bharathi, G. Basavaraju, Pramana. J. Phys. **39**, 297 (1992)
11. P. Mozejko, G. Karsperski, Cz. Szmytkowski, G.P. Karwasz, R.S. Brusa, A. Zecca, Chem. Phys. Lett. **257**, 309 (1996)
12. F.A. Gianturco, R.R. Lucchese, J. Chem. Phys. **108**, 6144 (1998)
13. R.J. Gulley, S.J. Buckman, J. Phys. B: At. Mol. Opt. Phys. **32**, L405 (1999)
14. M.H.F. Bettega, C. Winstead, V. McKoy, J. Chem. Phys. **112**, 8806 (2000)
15. Y. Jiang, J. Sun, L. Wan, Phys. Rev. A **62**, 2473 (2000)
16. H. Cho, R.J. Gulley, K. Sunohara, M. Kitajima, L.J. Uhlmann, H. Tanaka, S.J. Buckman, J. Phys. B: At. Mol. Opt. Phys. **34**, 1019 (2001)
17. H. Cho, R.J. Gulley, S.J. Buckman, J. Chin. Chem. Soc. **48**, 381 (2001)
18. D. Field, J.-P. Ziesel, S.L. Lunt, R. Parthasarathy, L. Suess, S.B. Hill, F.B. Dunning, R.R. Lucchese, F.A. Gianturco, J. Phys. B: At. Mol. Opt. Phys. **34**, 4371 (2001)
19. P. Carsky, R. Curik, F.A. Gianturco, R.R. Lucchese, M. Polasek, Phys. Rev. A **65**, 052713 (2002)
20. J. Sun, C. Du, Y. Liu, Phys. Lett. A **314**, 150 (2003)
21. C. Makochekanwa, O. Sueoka, M. Kimura, Phys. Rev. A **68**, 032707 (2003)
22. M. Kimura, C. Makochekanwa, O. Sueoka, J. Phys. B: At. Mol. Opt. Phys. **37**, 1461 (2004)
23. H.M. Boechat-Roberty, M.L.M. Rocco, C.A. Lucas, G.G.B. de Souza, J. Phys. B: At. Mol. Opt. Phys. **37**, 1467 (2004)
24. S. De-Heng, S. Jin-Feng, Z. Zun-Lue, L. Yu-Fang, Y. Chiang-Dong, Chin. Phys. **15**, 1278 (2006)
25. F. Blanco, G. García, Phys. Lett. A **360**, 707 (2007)
26. I. Iga, I.P. Sanches, E. de Almeida, R.T. Sugohara, L. Rosani, M.-T. Lee, J. Electron Spectrosc. Rel. Phenom. **155**, 14 (2007)
27. M.A. Er-Jun, M.A. Yu-Gang, C. Xiang-Zhou, F. De-Qing, S. Wen-Quing, T. Wen-Dong, Chin. Phys. Lett. **25**, 97 (2008)
28. I.P. Sanches, R.T. Sugohara, L. Rosani, M.-T. Lee, I. Iga, J. Phys. B: At. Mol. Opt. Phys. **41**, 185202 (2008)
29. H. Kato, M.C. Garcia, T. Asahina, M. Hoshino, C. Makochekanwa, H. Tanaka, Phys. Rev. A **79**, 62703 (2009)
30. H. Kato, M. Hoshino, H. Tanaka, P. Limão-Vieira, O. Ingólfsson, L. Campbell, M.J. Brunger, J. Chem. Phys. **134**, 134308 (2011)
31. G.L.C. de Souza, A.S. dos Santos, R.R. Lucchese, L.E. Machado, L.M. Brescansin, H.V. Manini, I. Iga, M.-T. Lee, Chem. Phys. **393**, 19 (2012)
32. S. Singh, R. Naghma, J. Kaur, B. Antony, J. Chem. Phys. **145**, 034309 (2016)
33. A.S. Barbosa, M.H.F. Bettega, J. Chem. Phys. **146**, 154302 (2017)

34. D. Prajapati, H. Yadav, P.C. Vinodkumar, C. Limbachiya, A. Dora, M. Vinodkumar, Eur. Phys. J. D **72**, 210 (2018)
35. M. Allan, R. Curik, P. Carsky, J. Chem. Phys. **151**, 064119 (2019)
36. F. Costa, L. Álvarez, A.I. Lozano, F. Blanco, J.C. Oller, M.H.F. Bettega, F. Ferreira da Silva, P. Limão-Vieira, G. García, J. Chem. Phys. **151**, 084310 (2019)
37. A.I. Lozano, F. Costa, X. Ren, A. Dorn, L. Álvarez, F. Blanco, P. Limão-Vieira, G. García, Int. J. Mol. Sci. **22**(9), 4601 (2021)
38. K. Takatsuka, V. McKoy, Phys. Rev. A **24**, 2473 (1981)
39. K. Takatsuka, V. McKoy, Phys. Rev. A **30**, 1734 (1984)
40. J. S. dos Santos, R. F. da Costa, M. T. do N. Varella, J. Chem. Phys **136**, 084307 (2012)
41. M.H.F. Bettega, L.G. Ferreira, M.A.P. Lima, Phys. Rev. A **47**, 1111 (1993)
42. R.F. da Costa, F.J. da Paixão, M.A.P. Lima, J. Phys. B: At. Mol. Opt. Phys. **38**, 4363 (2005)
43. A.G. Falkowski, M.A.P. Lima, F. Kossoski, J. Chem. Phys. **152**, 244302 (2020)
44. G.B. Bachelet, D.R. Hamann, M. Schlüter, Phys. Rev. B **26**, 4199 (1982)
45. R. F. da Costa, M. T. do N. Varella, M. H. F. Bettega, M. A. P. Lima, Eur. Phys. J. D **69**, 159 (2015)
46. G.M. Barca et al., J. Chem. Phys. **152**, 154102 (2020)
47. M.H.F. Bettega, Phys. Rev. A **81**, 062717 (2010)
48. T.H. Dunning Jr., J. Chem. Phys. **53**, 2823 (1970)
49. B.M. Bode, M.S. Gordon, J. Mol. Graph. Model. **16**, 133 (1998)
50. William J. Hunt, W.A. Goddard, Chem. Phys. Lett. **3**, 414 (1969)
51. J.F. Stanton, R.J. Bartlett, J. Chem. Phys. **98**, 7029 (1993)
52. O. Christiansen, H. Koch, P. Jørgensen, J. Chem. Phys. **103**, 7429 (1995)
53. H. Koch, O. Christiansen, P. Jørgensen, A.M. Sanchez de Merás, T. Helgaker, J. Chem. Phys. **106**, 1808 (1997)
54. D.G.A. Smith, L.A. Burns, A.C. Simmonett, R.M. Parrish, M.C. Schieber, R. Galvelis, P. Kraus, H. Kruse, R. Di Remigio, A. Alenaizan, A.M. James, S. Lehtola, J.P. Misiewicz, M. Scheurer, R.A. Shaw, J.B. Schriber, Y. Xie, Z.L. Glick, D.A. Sirianni, J.S. O'Brien, J.M. Waldrop, A. Kumar, E.G. Hohenstein, B.P. Pritchard, B.R. Brooks, H.F. Schaefer, AYu. Sokolov, K. Patkowski, A.E. DePrince, U. Bozkaya, R.A. King, F.A. Evangelista, J.M. Turney, T.D. Crawford, C.D. Sherrill, J. Chem. Phys. **152**, 184108 (2020)
55. CFOUR, a quantum chemical program package written by J.F. Stanton, J. Gauss, L. Cheng, M.E. Harding, D.A. Matthews, P.G. Szalay with contributions from A.A. Auer, R.J. Bartlett, U. Benedikt, C. Berger, D.E. Bernholdt, Y.J. Bomble, O. Christiansen, F. Engel, R. Faber, M. Heckert, O. Heun, C. Huber, T.-C. Jagau, D. Jonsson, J. Jusélius, K. Klein, W.J. Lauderdale, F. Lipparini, T. Metzroth, L.A. Mück, D.P. O'Neill, D.R. Price, E. Prochnow, C. Puzzarini, K. Ruud, F. Schiffmann, W. Schwalbach, C. Simmons, S. Stopkowicz, A. Tajti, J. Vázquez, F. Wang, J.D. Watts and the integral packages MOLECULE (J. Almlóf and P.R. Taylor), PROPS (P.R. Taylor), ABACUS (T. Helgaker, H.J. Aa. Jensen, P. Jørgensen, and J. Olsen), and ECP routines by A. V. Mitin and C. van Wüllen. For the current version, see http://www.cfour.de
56. D.A. Matthews, L. Cheng, M.E. Harding, F. Lipparini, S. Stopkowicz, T.-C. Jagau, P.G. Szalay, J. Gauss, J.F. Stanton, J. Chem. Phys. **152**, 214108 (2020)
57. T.N. Rescigno, B.I. Schneider, Phys. Rev. A **45**, 2894 (1992)
58. R.F. da Costa, M.H.F. Bettega, M.A.P. Lima, M.C.A. Lopes, L.R. Hargreaves, G. Serna, M.A. Khakoo, Phys. Rev. A **85**, 062706 (2012)
59. R. F. da Costa, M. H. F. Bettega, M. T. do N. Varella, E. M. de Oliveira, M. A. P. Lima, Phys. Rev. A **90**, 052707 (2014)
60. R. F. da Costa, E. M. de Oliveira, M.H. F. Bettega, M. T. do N. Varella, D.B. Jones, M.J. Brunger, F. Blanco, R. Colmenares, P. Limão-Vieira, G. García, M.A.P. Lima, J. Chem. Phys **142**, 104304 (2015)
61. R.F. da Costa, M. T. do N. Varella, M.H.F. Bettega, R.F.C. Neves, M.C.A. Lopes, F. Blanco, G. García, D.B. Jones, M.J. Brunger, M.A.P. Lima, J. Chem. Phys. **144**, 124310 (2016)
62. D.B. Jones, R.F.C. Neves, M.C.A. Lopes, R.F. da Costa, M. T. do N. Varella, M.H.F. Bettega, M.A.P. Lima, G. García, P. Limão-Vieira, M.J. Brunger, J. Chem. Phys **144**, 124309 (2016)
63. D.B. Jones, F. Blanco, G. García, R.F. da Costa, F. Kossoski, M. T. do N. Varella, M.H.F. Bettega, M.A.P. Lima, R.D. White, J. Brunger, J. Chem. Phys **147**, 244304 (2017)
64. D.B. Jones, R.F. da Costa, F. Kossoski, M.TDo.N. Varella, M.H.F. Bettega, F.F. da Silva, P. Limão-Vieira, G. García, M.A.P. Lima, R.D. White, M.J. Brunger, J. Chem. Phys. **148**, 124312 (2018)
65. R.F. da Costa, J.C. Ruivo, F. Kossoski, MTdoN. Varella, M.H.F. Bettega, D.B. Jones, M.J. Brunger, M.A.P. Lima, J. Chem. Phys. **149**, 174308 (2018)
66. G.M. Moreira, F. Kossoski, M.H.F. Bettega, RFd. Costa, J. Phys. B: At., Mol. Opt. Phys. **53**, 085002 (2020)
67. G.M. Moreira, M.H.F. Bettega, RFd. Costa, J. Appl. Phys. **129**, 203301 (2021)
68. P.-F. Loos, F. Lipparini, M. Boggio-Pasqua, A. Scemama, D. Jacquemin, J. Chem. Theory Comput. **16**, 1711 (2020)
69. N. Nakashima, M. Sumitani, I. Ohmine, K. Yoshihara, J. Chem. Phys. **72**, 2226 (1980)
70. N. Nakashima, K. Yoshihara, J. Chem. Phys. **77**, 6040 (1982)
71. Y. Li, J. Wan, X. Xu, J. Comput. Chem. **28**, 1658 (2007)
72. Y.-K. Kim, M.E. Rudd, Phys. Rev. A **50**, 3954 (1994)
73. H. Tanaka, M.J. Brunger, L. Campbell, H. Kato, M. Hoshino, A.R.P. Rau, Rev. Mod. Phys. **88**, 025004 (2016)
74. Y.-K. Kim, K. K. Irikura, M. E. Rudd, M. A. Ali, P. M. Stone, J. Chang, J. S. Coursey, R. Dragoset, A. R. Kishore, K. J. Olsen, A. Sansonetti, G. Wiersma, D. Zucker, M. Zucker, Electron-impact ionization cross section for ionization and excitation database (version 3.0), [Online]. Available: http://physics.nist.gov/ionxsec [2021, September 1]. National Institute of Standards and Technology, Gaithersburg, MD. (2004)

75. O. Sueoka, J. Phys. B: At. Mol. Opt. Phys. **21**, L631 (1988)